Pergamon

Journal of Structural Geology, Vol. 17, No. 9, pp. 1293 to 1302, 1995

0191-8141/95 $9.50+0.00

0191-8141(95)00029-1

Fault displacement-gradient folds and the structure at Lost Hills, California (U.S.A.)

JOHN WICKHAM

Department of Geology, University of Texas at Arlington, Arlington, TX 76019-0049, U.S.A.

(*Received* 19 *October* 1993; *accepted* 1 *March* 1995)

Abstract—Geometric models of fault-propagation folds require that the underlying fault tip propagate upward across layering. However, related folds can be generated if the tip remains stationary, or even moves back along the ramp as a pre-existing fault is reactivated. Fault-propagation folds, detachment folds, as well as those produced when there is no propagation are generated by a displacement gradient along the underlying fault, and, as a general class, can be called fault displacement-gradient folds. New geometric equations are derived which relate fold shape to displacement gradient, and fault-propagation folds are a special case of these more general equations. Growth sequences associated with these structures have been used to distinguish fault-propagation folds from fault-bend folds when the underlying structure is obscured. A displacement-gradient fold in which the fault tip retreats back down the ramp generates a growth sequence that in some cases could be confused with that of a fault-bend fold. The structure at Lost Hills, in the San Joaquin Valley of California (U.S.A.) has been interpreted as a fault-bend fold, but it may be a displacement-gradient fold which formed as a pre-existing fault was reactivated during a Pliocene change in plate motion.

INTRODUCTION

The purpose of this article is: (1) to suggest a new, more general name for certain types of fault-related folds; (2) to derive new geometric equations relating fold shape to fault displacement gradient, and (3) to apply the displacement-gradient model to a geologic example in which a reactivated fault tip may have migrated down a fault producing a growth sequence which could be confused with that produced by fault-bend folds (Suppe 1983).

Folds which are geometrically and mechanically related to faults have long been recognized using geologic criteria (Rich 1932). More recently, it has become clear that folding is also associated with earthquakes and the process of fault rupture (Stein & King 1984, Lin & Stein 1989, Berberian & Qorashi 1994). Folding of the topographic surface can be inverted to infer slip distribution and shape of the rupture zone of major earthquakes (King & Vita-Finzi 1980, Yielding *et al.* 1981, Ward & Barrientos 1986, Lin & Stein 1989).

Within the past 15 years, quantitative techniques pioneered by Suppe (1983) have been developed to relate the geometric properties of folds to the shape and displacement of related faults. Two general classifications of fault-related folds have emerged: fault-propagation folds (Fig. 1) and fault-bend folds (Fig. 2). In the former, folding is a consequence of a displacement gradient along the fault. In the latter, folding is a consequence of the non-planar shape of the fault.

Geometric models have traditionally been constrained by keeping both layer length and area constant during the transformation from the undeformed to the deformed state (Suppe 1983, 1985). Relaxing the constant bed length constraint (layer parallel simple shear)

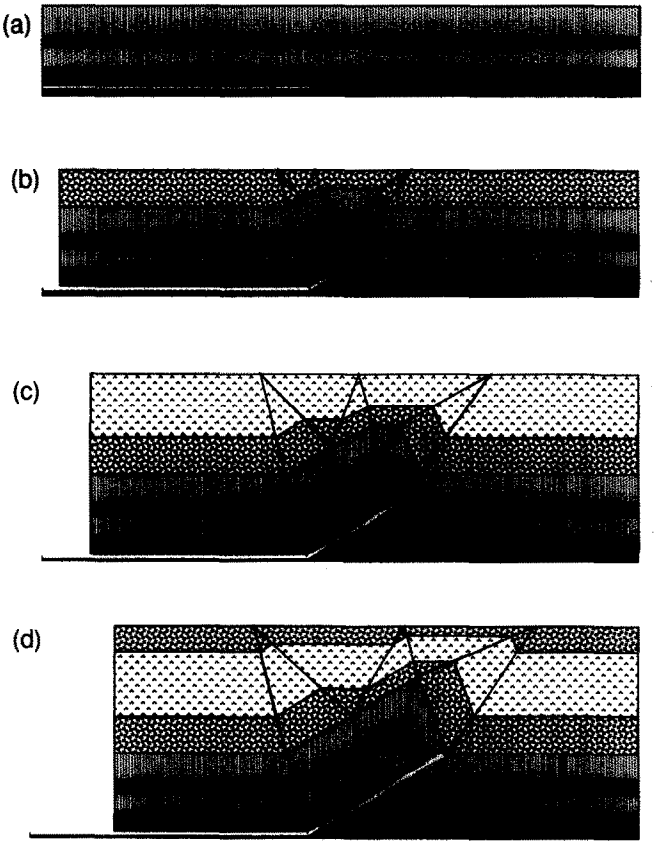

Fig. 1. Evolution of a traditional fault-propagation fold with a growth sequence produced by subsidence that exceeds fold amplitude growth. The growth sequence is shown in coarse patterns and the pre-growth sequence in fine patterns. A black circle marks the fault tip. The growth sequence over the backlimb consists of a flat stratigraphic panel between two dipping panels (b)–(d). This geometry does not occur in a fault-bend fold growth sequence. The growth stratigraphic section thins over the fold crest and is of normal thickness on the forelimb.

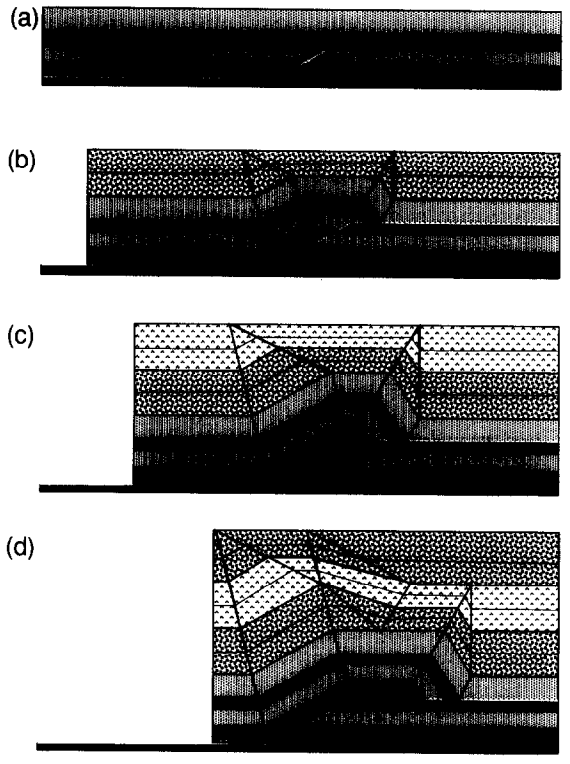

Fig. 2. Evolution of a fault-bend fold in which subsidence exceeds uplift of the fold. The growth sequence is shown in coarse patterns and the pre-growth sequence in fine patterns. Thinning of the growth sequence occurs over the forelimb and top of the underlying anticline (a)–(c) until fault displacement equals ramp length (c). Additional fault displacement produces stratigraphic thinning over the backlimb of the fold, and the crest of the fold in the growth sequence is displaced toward the backlimb of the fold in the pre-growth sequence (d).

tremendously increases the variety of geometric models and deformation histories that can be generated (Jamison 1987, Chester & Chester 1990, Mitra 1990, 1992). While geometric modeling is useful, physical laws (such as conservation of energy) are ignored, so any geometric model may be physically impossible.

Quantitative geometric fold models have proved extremely useful in interpreting near surface data, projecting structure to depth, and producing balanced cross-sections. This is especially true when sedimentation and folding are concurrent—e.g. the growth sequence (the sediment deposited during folding) may be used to distinguish fault-bend from fault-propagation folds, and to determine rates of folding, faulting and thrust history (Medwedeff 1989, Suppe *et al.* 1992, Zoetemeijer & Sassi 1992, Zoetemeijer *et al.* 1992).

Fault-propagation folds (Suppe 1985, Jamison 1987, Chester & Chester 1990, Suppe & Medwedeff 1990, Mitra 1990, 1992, Mosar & Suppe 1992) form because there is a displacement gradient along a fault ramp (Williams & Chapman 1983). This displacement gradient is related to, but not the same as, the slip/propagation distance ratio (*S/P*) defined by Williams & Chapman (1983) and emphasized by McNaught & Mitra (1993). The *S/P* ratio assumes that the slip is dissipated along the length of the fault. As such, the *S/P* ratio would be a minimum estimate of the displacement gradient which could be much higher if slip were dissipated only near one end of a fault.

DISPLACEMENT-GRADIENT FOLDS AND A NEW MODEL

A simple step fault-propagation model (Fig. 1) requires that the fault tip propagate up-section lengthening the ramp, but, if the constraint of constant bed length is removed, analogous folds can be generated even if the fault does not propagate (Fig. 3). Consequently, the name, fault-propagation fold, is not applicable to this model. A more appropriate name for a general class of folds, which would include fault-propagation folds as well as any fold occurring near a fault tip and related to dissipation of slip, would be fault displacement-gradient folds. This class would include a fold occurring near the tip of a bedding plane fault, of a high angle reverse fault, or of a ramp associated with a flat.

An example of an unusual reverse fault displacement-gradient fold model, which has some features similar to a fault-propagation fold, may occur when a pre-existing fault is reactivated, and its tip (the edge of zero displacement) moves back along the old fault leaving an inactive portion and an active portion with a displacement gradient (Fig. 4). This would most likely occur if there was a change in effective stress across a pre-existing fault. The difference between this fault displacement-gradient fold and the traditional fault-propagation fold is that the

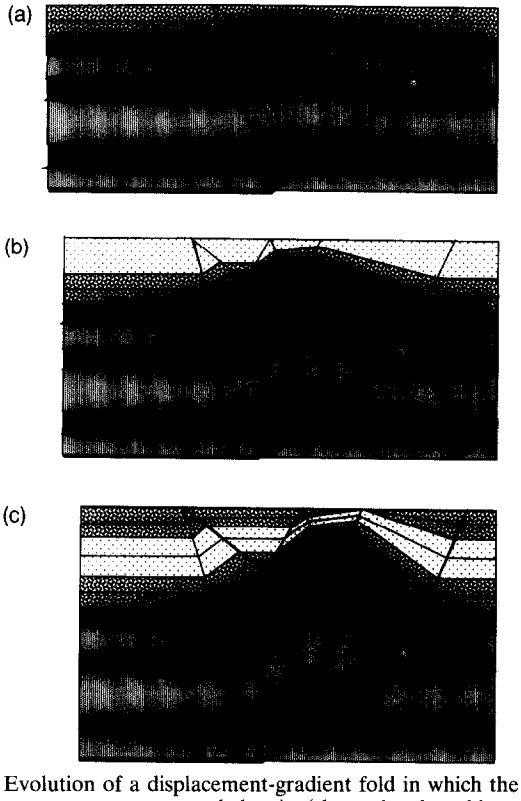

Fig. 3. Evolution of a displacement-gradient fold in which the fault ramp does not propagate, and the tip (shown by the white circle) remains stationary. The growth sequence is shown in coarse patterns and the pre-growth sequence in fine patterns. The backlimb growth sequence is similar to the traditional fault-propagation fold with a horizontal growth panel between two dipping ones. The forelimb growth sequence and fold crest is different from both the fault-propagation fold (Fig. 1) and fault-bend fold (Fig. 2) in that this displacement-gradient fold has wedge-shaped growth strata on the forelimb and the fold crest in the growth sequence has migrated toward the forelimb.

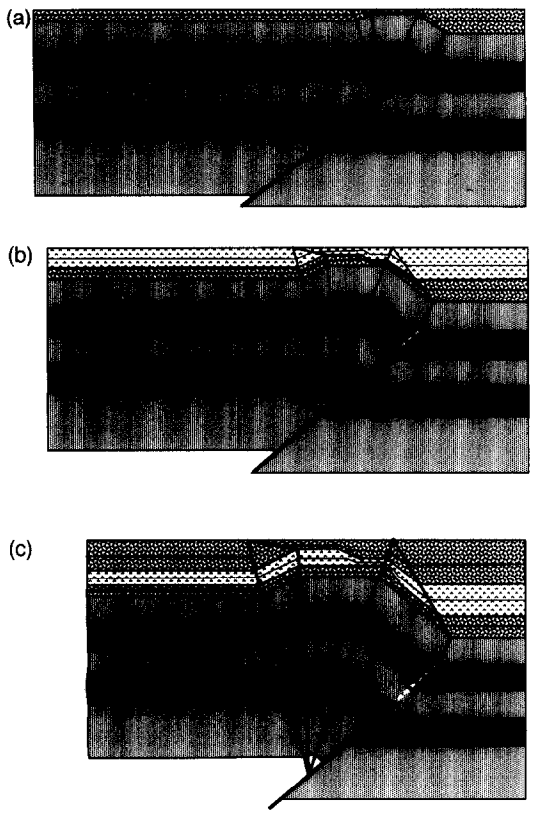

Fig. 4. Evolution of a reverse fault displacement-gradient fold in which a fault is reactivated and the tip moves downward as shown by the position of the black circle. The inactive part of the fault is dashed in (b) & (c). The growth sequence is shown in coarse patterns and the pre-growth sequence in fine patterns. The model presumes that the original fault was emergent, and no fault-related structures were present before reactivation. The model also presumes that any ramp–flat junction is too far away to effect the fold. The growth sequence over the backlimb does not contain the flat panel between two dipping ones typical of fault-propagation folds (Fig. 1), but resembles that of fault-bend folds (Fig. 2). Likewise the crest of the growth sequence lies on the backlimb side of the anticline, and the thin part of the growth sequence lies on the forelimb side. Because any ramp–flat junction is off the scale of this figure, strata of the pre-growth sequence are structurally higher behind the anticline than the pre-growth strata in front of the anticline. This also produces a thinner growth sequence behind the anticline than in front of it.

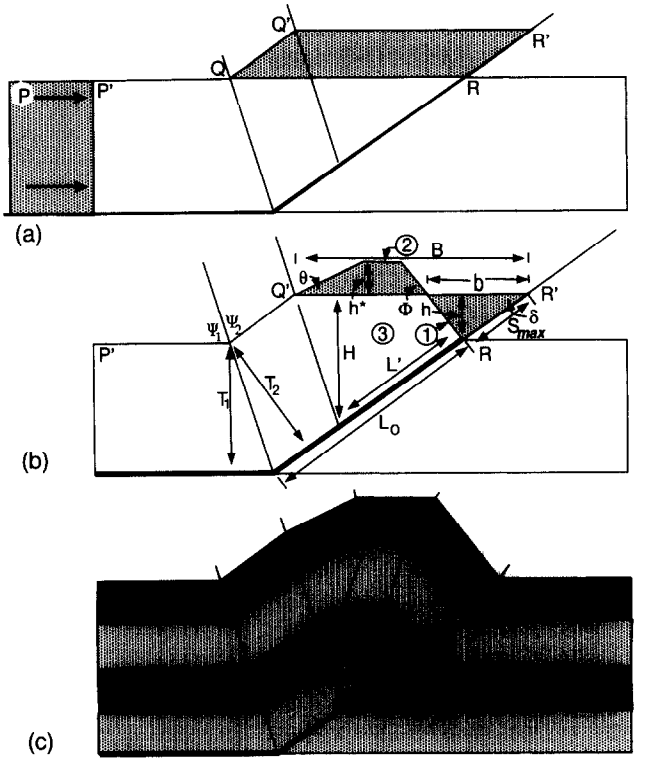

Fig. 5. Diagrams illustrating the graphical technique used to construct fault displacement-gradient folds. An explanation is in the text, and definitions of the variables are listed in Table 1.

fault tip of this model moves back along the pre-existing fault (Fig. 4) instead of propagating into unfaulted rock.

CONSTRUCTION OF FAULT DISPLACEMENT-GRADIENT FOLD MODELS

The fault displacement-gradient model presented here preserves area but not bed length. The geometric relationships are shown in Fig. 5. Figure 5(a) shows the displacement of the hanging wall as if there were no fault displacement gradient. Points P,Q and R move to points P′, Q′ and R′, and if area is conserved, the two patterned areas must be equal. Figure 5(b) assumes that displacement on the ramp dies out at the top of the model at point R. In this case, line Q′R′ is artificial and used only for construction purposes. The displacement gradient causes the upper surface to fold into line Q′R. To conserve area, trapezoid (2) must equal triangle (1) (Fig. 5b). Although other geometries are possible, using simple trapezoids makes it easier to establish relationships between the displacement gradient and the fold. Note that Trapezoid 2 (Fig. 5b) degenerates into a triangle when $b = B/2$ and $a = a^*$. In this case, the resulting geometry more closely resembles a traditional fault-propagation fold.

The variables used are listed in Table 1. The area of triangle (1) (Fig. 5b) can be related to the displacement gradient (∇) and area (A) of triangle (3):

$$a/A = hb/HB$$

However,

$$\text{Sin } \delta = h/S_{\max} = H/L_o,$$

so

$$h/H = S_{\max}/L_o = (1 - \nabla).$$

Therefore,

$$a = A(1 - \nabla)b/B. \quad (1)$$

Also,

$$a^* = h^*(B - b) - h^{*2}(\text{Cot } \Phi + \text{Cot } \Theta)/2. \quad (2)$$

To conserve area, $a = a^*$. However, Φ can be eliminated from equation (2) because

$$\text{Cot } \Phi = (b - S_{\max} \text{ Cos } \delta)/(S_{\max} \text{ Sin } \delta).$$

Equating equations (1) and (2) and eliminating Cot Φ results in the following relationship:

Table 1. Definitions of variables (see Fig. 5b)

L_0	Length of slip dissipation zone along fault
L'	Deformed length of material parallel to the slip dissipation zone
∇	Fault displacement gradient. $\nabla = L'/L_0$
S_{max}	Maximum slip along fault. $S_{max} = L_0(1 - \nabla)$
B	Undeformed length of folded line Q'R. Also the base of the triangle (3) with height H.
B'	Length of folded line Q'R
b	Base of small triangle (1)
h	Height of triangle (1)
h^*	Height of trapezoid (2)
H	Height of triangle (3)
δ	Dip angle of fault ramp
Φ	Dip angle of fold forelimb
Θ	Dip angle of upper part of fold backlimb
a	Area of triangle (1). $a = hb/2$
a^*	Area of trapezoid (2). $a^* = h^*(B - b) - h^{*2}(\mathrm{Cot}\Phi + \mathrm{Cot}\Theta)/2$
A	Area of triangle (3). $A = HB/2$
λ	Average layer parallel strain over the fold crest. $\lambda = B'/B$
T_1	Thickness of layer on one side of a fold hinge
T_2	Thickness of layer on the side of a fold hinge across from T_1
Ψ_1	Angle between fold hinge surface and layer on side T_1
Ψ_2	Angle between fold hinge surface and layer on side T_2

$$\frac{h^{*2} - 2h^*(B\text{-}b)S_{max}\,\mathrm{Sin}\,\delta}{b - S_{max}(\mathrm{Cos}\,\delta - \mathrm{Sin}\,\delta\,\mathrm{Cot}\,\Theta)} + \frac{2Ab(1 - \nabla)S_{max}\,\mathrm{Sin}\,\delta}{B[b - S_{max}(\mathrm{Cos}\,\delta - \mathrm{Sin}\,\delta\,\mathrm{Cot}\,\Theta)} = 0 \quad (3)$$

Equation (3) is a general relationship for fault displacement-gradient folds and can be solved for h knowing limb dips, fault dips, maximum slip, initial length and area of the folded layer, and the displacement gradient along the fault.

An average layer parallel strain over the crest of the model can also be calculated. If B' is the deformed layer length,

$$B' = B - b + S_{max}\,\mathrm{Sin}\,\delta/\mathrm{Sin}\,\Phi + h^*[\mathrm{Tan}(\Phi/2) + \mathrm{Tan}(\Theta/2)] \quad (4)$$

then average layer parallel strain λ is:

$$\lambda = B'/B = 1 - b/B + S_{max}\,\mathrm{Sin}\,\delta/(B\,\mathrm{Sin}\,\Phi) + h^*[\mathrm{Tan}(\Phi/2) + \mathrm{Tan}(\Theta/2)]/B. \quad (5)$$

A fold geometry based on equation (3) is shown in Fig. 5(c). There are several features in Fig. 5(c) which are different compared to the standard fault-propagation fold (Fig. 1): the flat crest is present in the core of the fold; hinge lines are curved; and two different dips are possible on the backlimb. [The terms backlimb and forelimb are used a little differently here than the usage recommended in the Glossary of Geology (Bates & Jackson 1987). Forelimb is used to refer to the limb of the fold nearest the fault tip, and backlimb refers to the limb farthest away from the fault tip no matter which is the steeper limb, or whether the fold is asymmetric or not.]

Equation (3) will also produce a simple step fault-propagation fold (Suppe & Medwedeff 1990) if $b = B/2$, ∇ = constant, $\Theta = \delta$, and $\lambda = 1$. Equation (3), however, does not include any layer parallel shear exerted on the hanging wall at the boundary of the model as in Suppe & Medwedeff (1990).

CHARACTERISTICS OF THE FOLD MODEL

Because the growth section of geometric models can be used to distinguish various types of fault-related folds, comparison of the growth sections in the various models is useful. There are also no constraints on layer thickness changes in either the forelimb or backlimb of the pre-growth strata. The dips of the fold limbs can change during folding, and limb thickening/thinning can also change with limb dip, and fold history. As with all kink folds the change in thickness across a kink hinge surface is proportional to the sine of the angle between layering and the hinge surface (see Fig. 5b); i.e.

$$T_1/\mathrm{Sin}\,\Psi_1 = T_2/\mathrm{Sin}\,\Psi_2 \quad (6)$$

where the subscripts refer to opposite sides of the hinge surface.

In the standard fault-propagation model (Fig. 1), the thinnest part of the growth stratigraphic section is in the triangular region spreading out above the hinge in the pre-growth strata (Fig. 1d), and growth strata thicken incrementally down the backlimb. Normal stratigraphic thickness occurs in the triangular region extending out from the forelimb, and a triangular wedge of horizontal layers occurs in the growth section above the backlimb in Fig. 1(d) (Suppe & Medwedeff 1990).

A fault displacement-gradient model (Fig. 3), in which the fault tip does not move, has a tapered forelimb growth section that thins towards the crest (Fig. 3a). As the fold grows, the hinge in the pre-growth strata migrates into the forelimb taper producing a crest in the growth section which is above the upper part of the forelimb of the underlying fold in the pre-growth strata (Figs. 3b & c). The growth section continues to thin over the crest of the pre-growth fold and then thickens down the backlimb (Figs. 3b & c). The wedge of horizontal strata that occurs in the fault-propagation fold (Fig. 1) is also present in the growth section of the backlimb.

Figure 4 is a reverse fault displacement-gradient model in which the fault tip moves down dip. A variation of this model is used for the geologic example in the next

section. In this model (Fig. 4), the fold crest in the pre-growth strata migrates toward the backlimb, opposite to the sense of displacement of the hangingwall in which it occurs. This produces a forelimb growth section with a triangular shaped region of thinned strata which changes over the crest into a normal thickness on the backlimb (Fig. 4c). Over the crest of the pre-growth fold, the growth strata has a more complex pattern of thickness changes. Note that the crest of the growth strata is displaced toward the backlimb relative to the crest in the pre-growth strata (Figs. 4b & c). The model shown in Fig. 4 is associated with a fault which does not flatten with depth in the vicinity of the fold. As a result, the hanging wall block is structurally higher than the footwall block, and the resulting growth section is thinner in the hanging wall than it is in the footwall.

Fault-bend folds (Fig. 2) have a growth section similar to the reverse fault displacement-gradient model of Fig. 4. Comparing the uppermost layer of Fig. 4(c) with Fig. 2(d), the crest of the growth section of both models is displaced toward the backlimb relative to the crest in the pre-growth strata; both models have a triangular shaped region of normal thickness above the backlimb giving way to thinner strata over the crest; both models have a triangular region of thinner strata above the forelimb which thickens to a normal section in front of the structure. There are also some differences between the two models. For example in the growth strata over the top of the structures, the displacement-gradient fold of Fig. 4 has more complicated stratigraphic thickness relationships over the crest of the pre-growth structure than the fault-bend fold does (Fig. 2). In addition, the displacement-gradient model (Fig. 4) has structural relief on the hanging wall because the ramp did not flatten in the vicinity of the fold. If there were a flat in the underlying fault, the back limb of Fig. 4 would have had a triangular region of horizontal strata in the growth section. The triangular region of horizontal strata is always absent in simple fault-bend folds.

While there are differences in the details of the growth section of the fault-bend fold and a reverse fault displacement-gradient model in which the fault tip moves down the ramp, these differences may be hard to detect in natural examples. The most obvious difference between the models in Figs. 2 and 4 is the structural relief in the displacement-gradient fold which is absent in the fault-bend fold of Fig. 2. Although it is possible to construct a double ramp fault-bend fold in which the front fold has apparent structural relief in the hanging-wall block, the presence or absence of this structural relief may be the easiest way to distinguish between this particular fault displacement-gradient model and simple fault-bend folds.

AN EXAMPLE FROM LOST HILLS, CALIFORNIA

The structure at Lost Hills, San Joaquin Valley, California (U.S.A.) (Fig. 6), is part of the Coast Ranges Foldbelt (Namson & Davis 1988), and has been used as an example of a fault-bend fold based mainly on the Plio-Pleistocene growth sequence across the structure (Medwedeff 1989). The approach used by Medwedeff (1989) is an excellent example of the use of geometric models to infer structural geometry at depth where information is unavailable (see also Mount *et al.* 1990).

Figure 7 is a seismic line across the Southeast Lost Hills structure. Seismic reflectors beneath the anticline are present down to approximately 3 s, but below that, the structure is not imaged. The growth sequence includes the Plio-Pleistocene Etchegoin, San Joaquin and Tulare Formations. At the level of the Upper Miocene Reef Ridge and Monterey Formations, the anticline has a broad crest, but at the level of the growth sequence the crest of the structure is located near the southwest limb of the lower level anticline. Note that the growth sequence is tapered over the northeast limb of the structure. The growth sequence is more or less consistent with a fault-bend fold model (Fig. 2) which led Medwedeff (1989, Fig. 4) to that interpretation. This interpretation of the structure has significant economic implications because the Monterey Formation near the surface produces petroleum. If Monterey also exists below an upper flat of a fault-bend fold, it could be an important exploration target.

While a fault-bend fold model fits the data reasonably well, the reverse fault displacement-gradient model (Fig. 4) also explains the available data, and resolves an important question concerning the fault-bend fold model: what happens to the fault displacement east of the structure where significant deformation is absent? In displacement-gradient structures all of the fault slip is accommodated by the folding.

Figure 8 is a cross-section constructed near the seismic line shown in Fig. 7. The cross-section is constrained by over 100 wells into the Monterey Formation in the crest of the structure, and a network of seismic lines (including Fig. 7). A deep well and linked seismic line (not shown) east of the structure constrains the formations in the footwall of the reverse fault. The seismic line of Fig. 7 does not include the North Belridge structure shown in Fig. 8. Also note that the vertical scale in Fig. 8 is in distance while it is time in Fig. 7.

Figure 9 presents one possible area-balanced geometric model for the kinematic development of the Lost Hills structure from the beginning of Monterey deposition (Fig. 9a) to the present (Fig. 9d). The reverse fault (Lost Hills Fault) was probably active during Monterey deposition (Fig. 9a). It may have been active earlier, but stratigraphic data from the lower Tertiary and Cretaceous in the Lost Hills area are not detailed enough to tell.

Displacement continued through Monterey, Reef Ridge and Lower Etchegoin time (Fig. 9b). The fault apparently cut the sea floor because a thinner stratigraphic sequence was deposited on the hanging-wall compared to the footwall (Fig. 8). No systematic change in thickness of these sediments occurs on the hanging-wall so there is no evidence of folding during Miocene

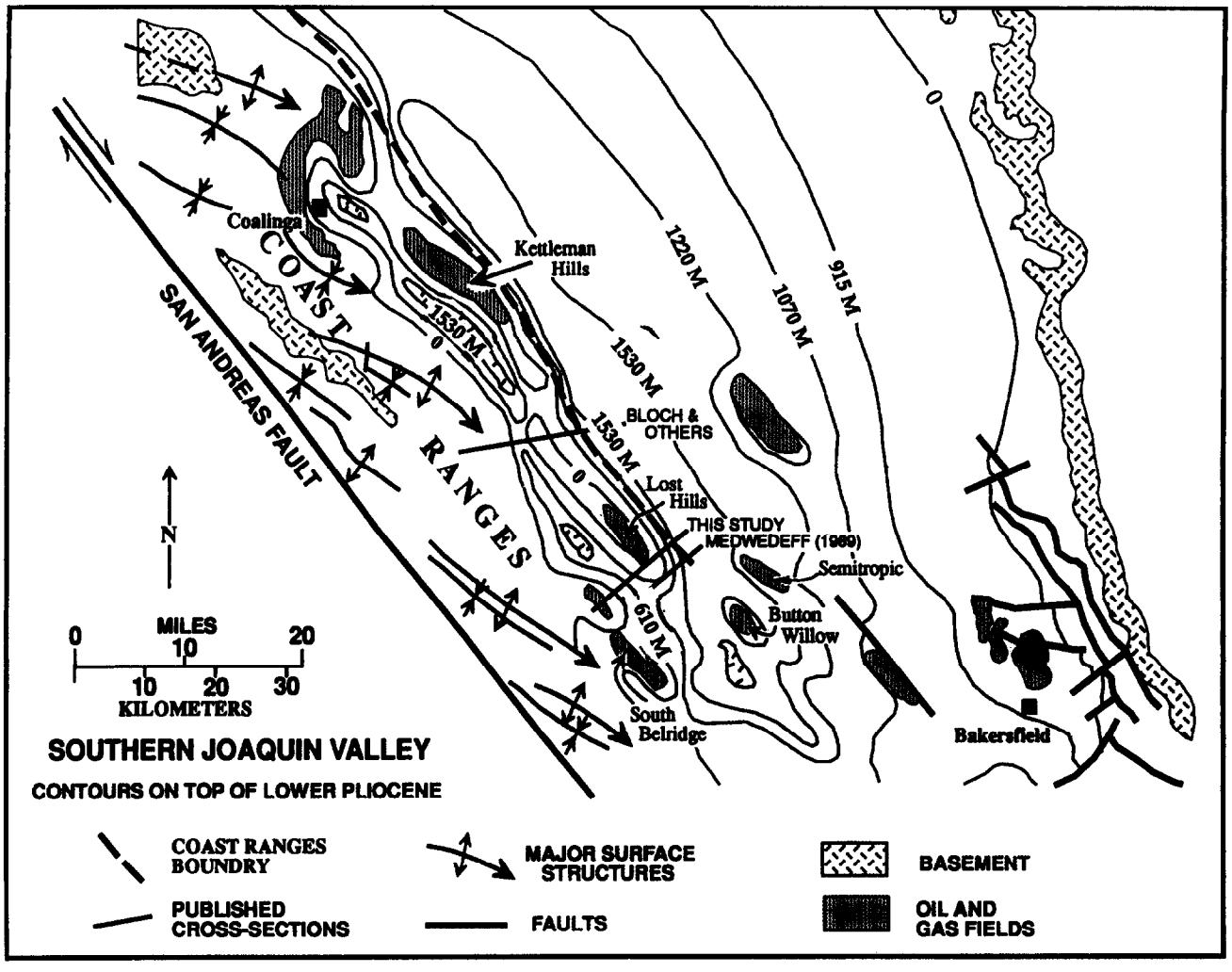

Fig. 6. Map of the southern San Joaquin Valley near Bakersfield, California (U.S.A.), showing location of the seismic line and cross-section shown in Figs. 7 and 8, as well as other published cross-sections referred to in the text.

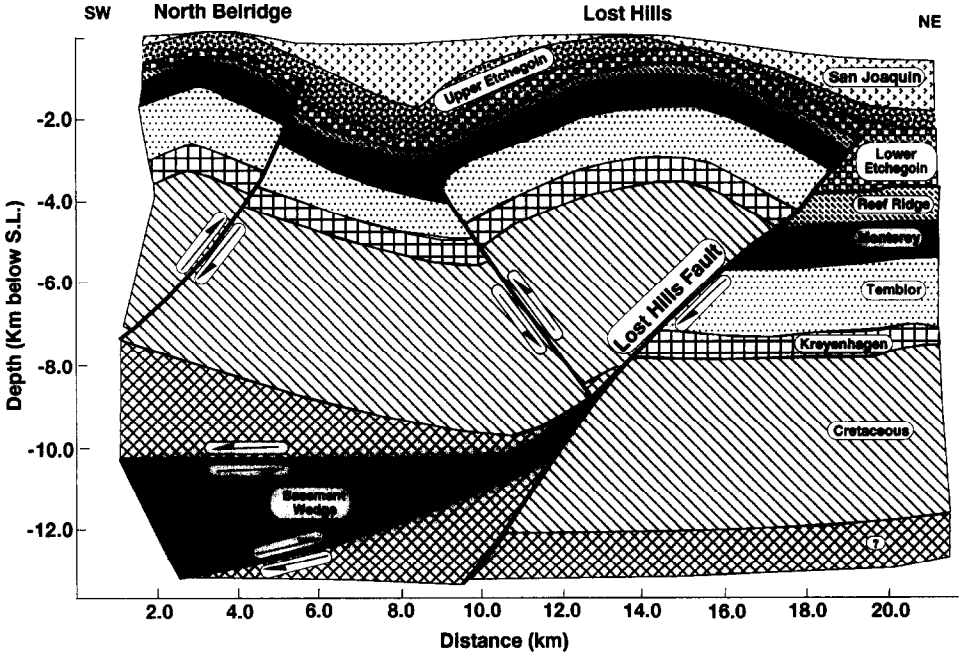

Fig. 8. A cross-section of the structure at Lost Hills based on a network of seismic lines (including Fig. 7), drill holes, and the geometric model shown in Fig. 9. (See Fig. 6 for location.)

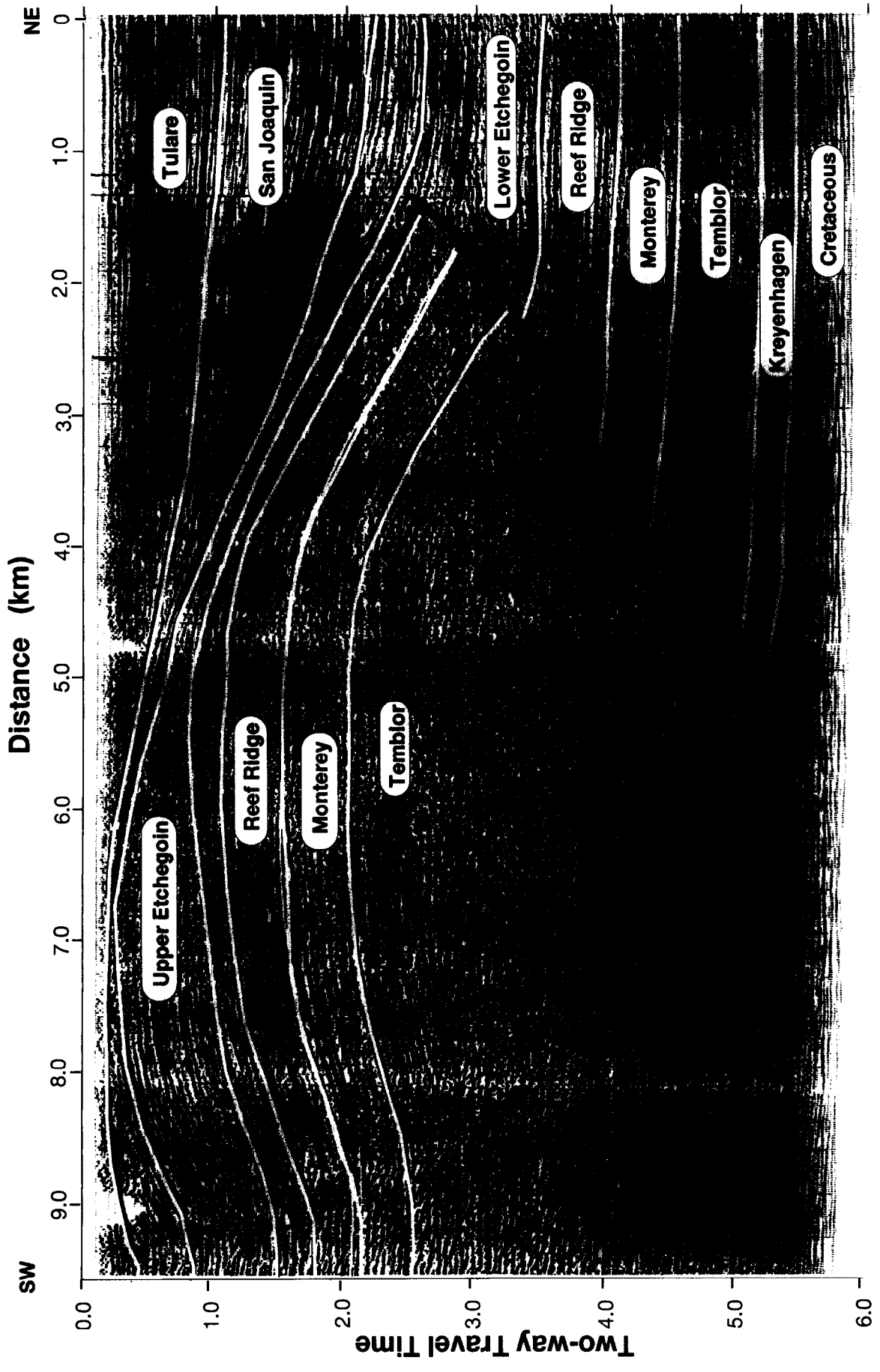

Fig. 7. Interpreted seismic line across the southern end of the Lost Hills structure (see Fig. 6 for location). The interpretation was also constrained by drill holes penetrating the Monterey over the anticline, a network of other seismic lines, and a deep drill hole to the North East (The Great Basins Well) that constrains the footwall.

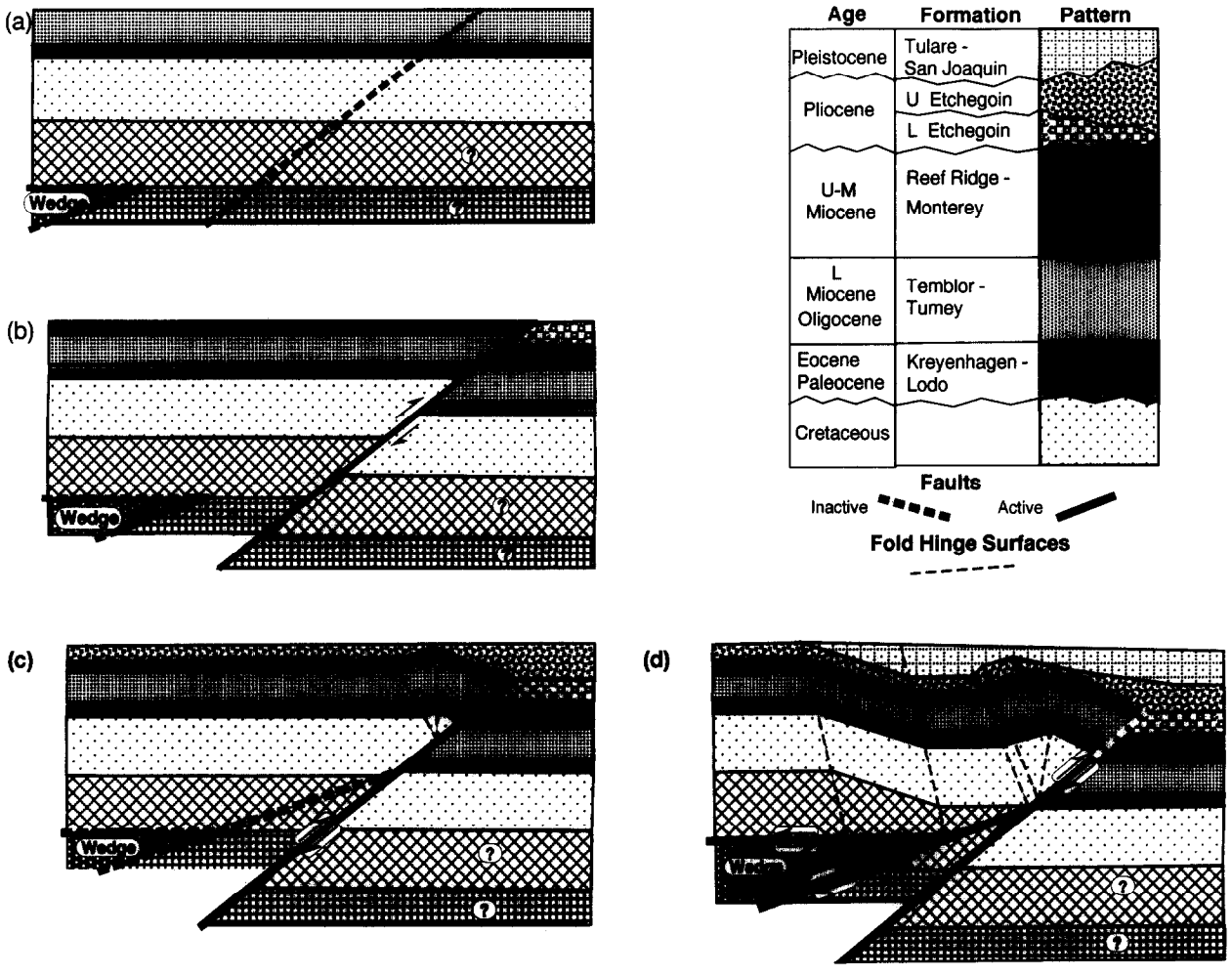

Fig. 9. A geometric model showing a possible history of the Lost Hills structure. Thick dashed lines represent inactive fault segments. Solid thick lines represent active fault segments. Further description is given in the text.

displacement on the fault. This requires a planar fault, with no displacement gradient, at least over the horizontal distance of the cross-section. There was obviously a vertical component of slip on this fault, but it could also have had a significant horizontal component as well. No geological information is available to determine the horizontal component.

By upper Etchegoin time (Fig. 9c), the Lost Hills Fault had apparently stopped growing and was covered by sediment. Thickness changes in the upper Etchegoin (Figs. 7 and 8) on the hanging-wall indicate that shortening was taken up by folding. This change from faulting to folding at Lost Hills coincided in time with the Pliocene change in relative motion between the Pacific and North America plates (Cox & Engebretsen 1985, Pollitz 1986, Montgomery 1993). If the modern stress field is representative of the Pliocene stress, horizontal shortening became nearly perpendicular to the fault (Mount & Suppe 1987, 1992, Zoback *et al.* 1987, Castillo & Zoback 1994). This may account for the fact that the fault stopped moving and was then reactivated. The fold that begins to form at this stage (Fig. 9c) can be modeled as a reverse fault displacement-gradient fold. The fold forms over an interval of diminishing displacement along the upper part of the fault.

In Fig. 9(d), the final stage, the fault tip moves farther down the fault, and the fold crest of the growth section migrates above the backlimb of the fold in the pre-growth section.

In the model (Fig. 9), wedging and low angle thrust faults at depth are not activated until the Early Pliocene change in plate motion and the deposition of the upper Etchegoin (Fig. 9c). In the interpretation of the deep structure, a thrust fault intersects the Lost Hills Fault and some of the thrust fault displacement is transferred to the steeper dipping fault to modify the Lost Hills fold and move its crest southwestward. At the same time, the geometry of and displacement on the deep thrust fault also needs to generate the NE-dipping panel of sediments between Lost Hills and North Belridge. A geometric wedge, with opposite sense of displacement on its floor and roof thrusts is the simplest explanation. Some of the displacement on the floor thrust is used to produce the Lost Hills fold. The rest of the displacement is accommodated by the roof thrust to generate the NE-dipping panel (Fig. 9d). This wedge may be a reacti-

vation of the older Cretaceous–Lower Tertiary wedge of Wentworth *et al.* (1984), or a new structure. However it seems to be a regional feature and also occurs at the northwest end of the Kettleman Hills of which the Lost Hills structure is a part (Bloch *et al.* 1993).

This reverse fault displacement-gradient fold is appropriate for preexisting faults which were reactivated with a change in effective stress. The sedimentary growth pattern fits the Lost Hills structure quite well (compare Figs. 9d and 7) and the model is consistent with the geological data. However, I know of no other cases reported in the literature where a fault tip and the related process zone of a fault, has migrated back along the fault, opposite to the direction of initial propagation. For this opposite migration to occur, there would have to be a change in the effective stress that initiated the fault in the first place. This change in effective stress may reactivate the fault, and the fault would probably be misoriented in the new stress field for unstable frictional sliding governed by a Coulomb failure criterion. Sibson *et al.* (1988) and Sibson (1990) have considered reactivation of misoriented faults and concluded that reactivation in stress fields conducive to thrust faulting requires a fluid pressure in excess of the lithostatic load. Therefore, the position of the fault rupture depends on the location of fluid pressure buildup that exceeds the lithostatic load. Migration of the reactivated fault tip down the fault would then depend on a mechanism that produced a zone of high fluid pressure that moved deeper with time. Although the history of high pore pressures is not known, they do exist at present in the vicinity of the Lost Hills structure (Yerkes *et al.* 1990).

SUMMARY AND CONCLUSIONS

Fault displacement-gradient folds can be modeled geometrically by maintaining constant area, but not necessarily constant layer length. The fault tip may propagate into unfaulted rock (fault-propagation folds), may not move at all, or may retreat back down the fault if the fracture is reactivated. A general equation is derived relating fold shape to fault displacement gradient, and fault-propagation folds are a special case.

The anticline near Lost Hills, California, U.S.A., has a growth sequence which has been interpreted as overlying a fault-bend fold. However, the reactivated reverse fault displacement-gradient fold model can also explain the growth sequence, and should be considered when interpreting structural history.

Finally, geometric models that conserve area and/or line length may be physically impossible because they do not conserve energy or account for material properties. To be plausible, however, it is necessary to find a natural example which is at least consistent with the geometric model.

Acknowledgements—Special thanks to G. Eisenstadt, M. B. Gray, J. Helwig, P. Hennings and C. W. Passchier for critical comments on earlier drafts of this paper, and to Mobil Research and Development Corp. and Mobil Exploration and Producing U.S. for funding and permission to publish.

REFERENCES

Bates, R. L. & Jackson, J. A. 1987. *Glossary of Geology*. American Geological Institute, Alexandria, VA.

Berberian, M. & Qorashi, M. 1994. Coseismic fault-related folding during the South Golbaf earthquake of November 20, 1989, in Southeast Iran. *Geology* **22**, 531–534.

Bloch, R., von Huene, R., Hart, P. & Wentworth, C. 1993. Style and magnitude of tectonic shortening normal to the San Andreas Fault across Pyramid Hills and Kettleman Hills South Dome, California. *Bull. geol. Soc. Am.* **105**, 464–478.

Castillo, D. A. & Zoback, M. D. 1994. Systematic Variations in Stress State in the Southern San Joaquin Valley: Inferences Based on Well-Bore Data and Contemporary Seismicity. *Bull. Am Ass. Petrol. Geol.* **78**, 1257–1275.

Chester, J. S. & Chester, F. M. 1990. Fault-propagation folds above thrusts with constant dip. *J. Struct. Geol.* **12**. 903–910.

Cox, A. & Engebretsen, D. 1985. Change in motion of Pacific Plate at 5 Myr BP. *Nature* **313**, 472–474.

Jamison, W. J. 1987. Geometric analysis of fold development in overthrust terrains. *J. Struct. Geol.* **9**, 207–219.

King, G. C. P. & Vita-Finzi, C. 1980. Active folding in the Algerian earthquake of 10 October 1980. *Nature* **292**, 22–26.

Lin, J. & Stein, R. S. 1989. Coseismic folding, earthquake recurrence, and the 1987 source mechanism at Whittier Narrows, Los Angeles Basin, California. *J. geophys. Res.* **94**, 9614–9632.

McNaught, M. A. & Mitra, G. 1993. A kinematic model for the origin of footwall synclines. *J. Struct. Geol.* **15**, 805–808.

Medwedeff, D. A. 1989. Growth fault-bend folding at Southeast Lost Hills, San Joaquin Valley, California. *Bull. Am. Ass. Petrol. Geol.* **73**, 54–67.

Mitra, S. 1990. Fault-propagation folds: geometry, kinematic evolution, and hydrocarbon traps. *Bull. Am. Ass. Petrol. Geol.* **74**, 921–945.

Mitra, S. 1992. Balanced Structural Interpretation in fold and thrust belts. In: *Structural Geology of Fold and Thrust Belts* (edited by Mitra, S. & Fisher, G. W.). The Johns Hopkins University Press, Baltimore, 54–77.

Montgomery, D. R. 1993. Compressional uplift in the central California Coast Ranges. *Geology* **21**, 543–546.

Mosar, J. & Suppe, J. 1992. Role of shear in fault-propagation folding. In: *Thrust Tectonics* (edited by McClay, K. R.). Chapman and Hall, London, 123–132.

Mount, V. S. & Suppe, J. 1987. State of stress near the San Andreas fault: Implication for wrench tectonics. *Geology* **15**, 1143–1146.

Mount, V. S. & Suppe, J. 1992. Present-day stress orientation adjacent to active strike-slip faults: California and Sumatra. *J. geophys. Res.* **97**, 11,995–12,013.

Mount, V. S., Suppe, J. & Hook, S. C. 1990. A forward modeling strategy of cross-sections. *Bull. Am. Ass. Petrol. Geol.* **74**, 521–531.

Namson, J. S. & Davis, T. 1988. Seismically active fold-and-thrust belt in the San Joaquin Valley, Central California. *Bull. geol. Soc. Am.* **100**, 257–273.

Pollitz, F. F. 1986. Pliocene change in Pacific Plate motion. *Nature* **320**, 738–741.

Rich, J. L. 1932. Mechanics of low-angle overthrust faulting as illustrated by Cumberland thrust block, Virginia, Kentucky, and Tennessee. *Bull. Am. Ass. Petrol. Geol.* **18**, 1584–1596.

Sibson, R. H. 1990. Rupture nucleation on unfavorably oriented faults. *Bull. Seism. Soc. Am.* **80**, 1580–1604.

Sibson, R. H., Robert, F. & Poulsen, H. 1988. High-angle reverse faults, fluid-pressure cycling, and mesothermal gold–quartz deposits. *Geology* **16**, 551–555.

Stein, R. S. & King, G. C. P. 1984. Seismic potential revealed by surface folding; 1983 Coalinga, California earthquake. *Science* **224**, 869–872.

Suppe, J. 1983. Geometry and kinematics of fault-bend folding. *Am. J. Sci.* **283**, 684–721.

Suppe, J. 1985. *Principles of Structural Geology*. Prentice-Hall, Inc., Englewood Cliffs, N.J.

Suppe, J. & Medwedeff, D. A. 1990. Geometry and Kinematics of fault-propagation folding. *Ecolg. geol. Helv.* **83**, 409–454.

Suppe, J., Chou, G. T. & Hook, S. C. 1992. Rates of folding and faulting determined from growth strata. In: *Thrust Tectonics* (edited by McClay, K. R.). Chapman and Hall, London, 105–122.

Ward, S. N. & Barrientos, S. E. 1986. An inversion for slip distribution and fault shape from geodetic observations of the 1983, Borah Peak, Idaho, earthquake. *J. geophys. Res.* **91**, 4909–4919.

Wentworth, C. M., Blake, M. C. Jr., Jones, D. L., Walter, A. W. & Zoback, M. D. 1984. Tectonic wedging associated with emplacement of the Franciscan assemblage, California Coast Ranges. In: *Franciscan Geology of Northern California* (edited by Blake, M. C. Jr.). *Pacific Section SEPM* **43**, 163–173.

Williams, G. & Chapman, T. 1983. Strains developed in the hanging-walls of thrusts due to their slip/propagation rate: a dislocation model. *J. Struct. Geol.* **5**, 563–571.

Yerkes, R. F., Levine, P. & Wentworth, C. M. 1990. Abnormally high fluid pressures in the region of the Coalinga earthquake sequence and their significance. *Prof. Pap. U.S. geol. Surv.* **12487**, 235–257.

Yielding, G., Jackson, J. A., King, G. C. P., Sinvhal, H., Vita-Finzi, C. & Wood, R. M. 1981. Relations between surface deformation, seismicity, rupture characteristics and fault geometry during the El Asnam (Algeria) earthquake of 10 October 1980. *Earth & Planet. Sci. Lett.* **56**, 287–304.

Zoback, M. D., Zoback, M. L., Mount, V. S., Suppe, J., Eaton, J. P., Healy, J. H., Oppenheimer, D. H., Reasenberg, P. A., Jones, L. M., Raleigh, B. C., Wong, I. G., Scotti, O. & Wentworth, C. M. 1987. New evidence on the state of stress of the San Andreas fault system. *Science* **238**, 1105–1111.

Zoetemeijer, R. & Sassi, W. 1992. 2-D reconstruction of thrust evolution using the fault-bend fold method. In: *Thrust Tectonics* (edited by McClay, K. R.). Chapman and Hall, London, 133–140.

Zoetemeijer, R., Sassi, W., Roure, F. & Cloetingh, S. 1992. Stratigraphic and kinematic modeling of thrust evolution, northern Apennines, Italy. *Geology* **20**, 1035–1038.